Photocatalytic degradation of acetone, acetaldehyde and toluene in gas-phase: Comparison between nano and micro-sized TiO$_2$

C.L. Bianchi [a,*], S. Gatto [a], C. Pirola [a], A. Naldoni [b], A. Di Michele [c], G. Cerrato [d], V. Crocellà [d], V. Capucci [e]

[a] Università degli Studi di Milano, Dipartimento Chimica, Via Golgi 19, 20133 Milano (Italy) & Consorzio INSTM, 50121 Firenze Italy
[b] CNR–Istituto di Scienze e Tecnologie Molecolari, Via Golgi 19, 20133 Milano, Italy
[c] Università degli Studi di Perugia, Dipartimento Fisica, Via Pascoli, 06123 Perugia Italy
[d] Università degli Studi di Torino, Dipartimento Chimica & NIS Centre of Excellence, Via Giuria 7, 10125 Torino (Italy) & Consorzio INSTM, 50121 Firenze Italy
[e] GranitiFiandre SpA, Via Radici Nord 112, 42014 Castellarano Italy

ARTICLE INFO

ABSTRACT

Volatile organic compounds (VOCs) are prevalent components of indoor air pollution. The photocatalytic degradation could be an interesting method to degrade them.

This paper reports the photoactivity study of two classical nano-sized and two micro-sized commercial TiO$_2$ powdered samples. Photocatalytic tests have been performed following the degradation of acetone, acetaldehyde and toluene in the gas phase under UV light. An accurate study of the intermediate oxidation products was performed. XPS and FTIR analyses allowed to highlight the relationship between TiO$_2$ surface properties and reactivity toward VOCs explaining the different behavior of the photocatalyst in case of hydrophilic and hydrophobic pollutants.

1. Introduction

Past and recent literature is full of new synthesis routes to prepare tailored nano-TiO$_2$ in order to enhance the photocatalytic efficiency of such material [1–3]. The aim is to reduce the particles dimension toward the very small nano-sized (few nanometers), to allow the preparation of very photoactive TiO$_2$ with complex and tailored shapes and also to obtain a powdered sample with particles all of the same size avoiding the mixture of big size and ultrafine.

However this scientific run does not take into account the possibility that nano-sized materials could be dangerous for the human health. Many papers were recently published on this topic [4–7]. Brun et al. showed the in vitro evidence of disruption of the blood-brain barrier function after acute and repeated/long-term exposure to TiO$_2$ nanoparticles [8]. Green et al. noted that the scientific community is faced with the challenge of developing new risk assessment methodologies capable of identifying

exposure characteristics and adverse effects of engineered nanoparticles [9].

It is well know that TiO$_2$ is not toxic by its chemical nature and it is also true that nanoparticles tend to aggregate in some environments, including biological environment, to form clusters of a bigger size [10]. The main question is if it is necessary the use of nano-sized particles in an exclusive way. Kwon et al. stated that nanocatalysts having small particle size, high surface area, and a high density of surface coordination unsaturated sites offer improved catalytic performance over microscale catalysts but this does not imply the impossibility a priori to use these latter in selected conditions [11].

The main target of the present paper is to identify possible features of large-sized TiO$_2$ particles so to exclude a priori their use in photocatalysis or, vice versa, to highlight similarities between nano and larger-sized samples to identify a possible role of larger size particles especially in formulations. Therefore, the photocatalytic behavior of four commercial powdered TiO$_2$ was compared. Two samples were well-known benchmark TiO$_2$ chosen among all the commercially available nano-sized photoactive TiO$_2$. The other two materials were chosen among the commercial

* Corresponding author. Tel.: +39 0250314253; fax: +39 0250314300.
E-mail address: claudia.bianchi@unimi.it (C.L. Bianchi).

titania-based pigmentary products having some specific features: pure anatase polymorph, particle size over 100 nm (micro-sized), absence of ultrafine particles (nano-sized particles), no specific post-treatment at the material surface to stabilize it after the preparation, no addition of dopants.

An exhaustive characterization from both the surface and structural point of view of the materials was coupled to the investigation of the photocatalytic efficiency of these four samples to degrade three different VOCs in the gas phase: acetone, acetaldehyde and toluene, chosen as they are specific molecules for indoor pollution. Acetone and acetaldehyde follow the same degradation pathway while toluene, also due to the presence of the aromatic ring, exhibits a more complicated path with the formation of byproducts which can be considered pollutants themselves and thus to degrade in turn.

In the case of toluene, various adsorbed aromatic species (benzoic acid, hydroquinone, benzyl alcohol, benzaldehyde, and cresols) were monitored by analyzing the samples surface after the kinetic runs by means of Fourier transform infrared (FTIR) spectroscopy.

2. Experimental

Acetone, acetaldehyde and toluene are all Fluka products at high purity grade.

Four commercial TiO₂ samples were selected without further treatment before their characterization and use. Two by Cristal (PC105 and AT-1), one by Kronos (1077) and one by Evonik (P25), always used as photocatalytic reference material.

2.1. Samples characterization

The surface area of all catalysts was determined by conventional N_2 adsorption (BET) at 77 K using a Sorptometer instrument (Costech Mod. 1042).

X-ray photoelectron spectra (XPS) were taken in an M-probe apparatus (Surface Science Instruments). The source was monochromatic Al Kα radiation (1486.6 eV). The accuracy of the reported BE can be estimated to be ±0.2 eV.

The crystalline nature of the samples was investigated by X-ray diffraction (XRD) using a PW3050/60 X'Pert PRO MPD diffractometer from PAN analytical working Bragg-Brentano, using as source the high power ceramic tube PW3373/10 LFF with a Cu anode equipped with Ni filter to attenuate Kβ. Scattered photons have been collected by a RTMS (Real Time Multiple Strip) X'celerator detector. The calculation of the crystallite size is given by the Scherrer equation: $t = 0.9\lambda/(\beta_{hkl} \times \cos\theta_{hkl})$, where t is the crystallite size, λ is the X-ray wavelength of radiation for CuKβ, β_{hkl} is the full-width at half maximum (FWHM) at (hkl) peak and θ_{hkl} is the diffraction angle.

The morphology of the catalysts was inspected by means of high resolution electron transmission microscopy (HR-TEM) and scanning electron microscopy (SEM). TEM images were recorded using a JEOL 3010-UHR instrument (acceleration potential: 300 kV; LaB₆ filament). Samples were "dry" dispersed on lacey carbon Cu grids. High resolution SEM images were acquired by a FEG LEO 1525, at the acceleration voltage of 15 kV by inlens detector and with magnifications of 250,000 and 500,000. The samples were sputter-coated with chrome at 120 mA for 25 s.

FTIR spectra in the mid-infrared region were obtained at 4 cm^{-1} resolution on a Bruker IFS28 spectrophotometer equipped with MCT cryodetector. All samples were examined in situ in the form of self-supporting pellets ($\sim$20 mg cm^{-2}) and mechanically protected with a pure gold frame. The spectra were obtained with the solid sample contained in a home-made quartz cell, equipped with KBr windows, connected to a conventional high-vacuum line

(UHV) that allows samples activation and spectra acquisition on the materials of interest in strictly in situ conditions.

For the characterization of the light absorption features and band-gap determinations, diffuse reflectance spectra (DRS) of the powders were collected on a UV–vis scanning spectrophotometer (PerkinElmer, Lambda 35), which was equipped with a diffuse reflectance accessory. A TiO₂ thin film was placed in the sample holder on integrated sphere for the reflectance measurements. A "total white" PerkinElmer reference material was used as the reference. Data were elaborated using the Kubelka–Munk equation [12].

2.2. Photocatalytic setup

The photocatalytic efficiency was monitored following the degradation of three different VOCs: acetone, acetaldehyde and toluene. The setup was precisely described elsewhere [13] operating in static condition. Photocatalytic degradations were conducted in a Pyrex glass cylindrical reactor with diameter of 200 mm and effective volume of 5 L. The amount of catalyst (in the form of powder deposited from 2-propanol slurry on flat glass disk) used in the tests was 0.05 g [14]. The gaseous mixture in the reactor was obtained by mixing hot chromatographic air (f.i. 250 °C for toluene), humidified at 40%, and a fixed amount of volatilized pollutant, in order to avoid condensation. The initial concentration of VOCs in the reactor was 400 ppmv. Photon sources were provided by a 500 W iron halogenide lamp (Jelosil, model HG 500) emitting in the 315–400 nm wavelength range (UV-A) at 30 Wm^{-2}. Acetone and acetaldehyde tests lasted for 2 h; 6 h for toluene due to the difficulty in degrading a molecule with an aromatic ring. The actual concentration of pollutant in the reactor was determined directly by micro-GC sampling.

Toluene and all its intermediate oxidation products were determined directly investigating the sample surface after the kinetic run by FTIR spectroscopy. The determination of CO₂ by gas chromatography was also performed.

3. Results and discussion

The present work reports some significantly different aspects with respect to the major part of literature data. The first aspect concerns the use of micro-size TiO₂ samples as already discussed in the Introduction and the comparison between their photoactivity with respect to the classical nano-crystallites materials. Two large-size, high-purity, commercial anatase samples (1077 and AT-1) are here considered.

A second aspect regards the pollutant level in the reacting chamber. The major part of literature results pertain to several hundred parts per billion (ppb) levels or to a few parts per million (ppm) [15–18]. In this work, significantly higher VOCs levels (400 ppm) were adopted in order to bring to light catalyst deactivation processes on a short time scale, to precisely identify the nature of the reaction intermediates and also to evaluate the possible feasibility of a photocatalytic degradation process even in severe pollution conditions on sample of different crystallite sizes.

3.1. Surface, structural and morphological characterization

The XRD patterns relative to the four selected samples are reported in Fig. 1. Anatase is the unique polymorph present for all samples, except for the well-known P25 which exhibits the phase composition 80:20 in anatase/rutile ratio. The crystallographic reflexes (1 0 1), (2 0 0) and (2 1 1) have been employed to calculate the average crystallites size of the various titania particles (Table 1, third column). P25 and P105 have comparable crystallite size centered at around 25 nm, while the samples 1077 and AT-1

Table 1
Main features of the selected TiO$_2$ sample.

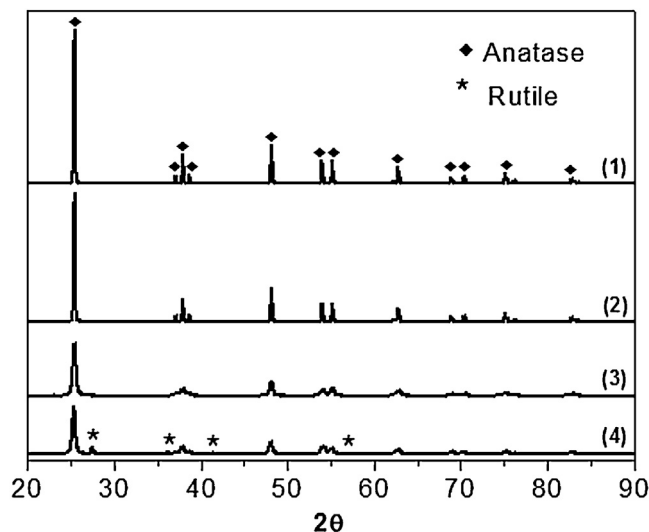| Sample	BET surface area (m^{2}g^{-1})	Average crystallites size (nm)	XPS Ti 2p$_{3/2}$ (eV)	XPS OH/O$_{tot}$	Band Gap (eV)
P25	50	26	458.4	0.14	3.21
PC105	80	23	458.4	0.85	3.19
1077	12	130	458.3	0.32	3.15
AT-1	12	192	458.3	0.24	3.15

Fig. 1. XRD patterns of AT-1 (1), 1077 (2), PC105 (3) and P25 (4).

have values of 130 and 192 nm, respectively. These structural properties are reflected in the BET surface area of micro-sized samples (1077 and AT-1) which is much lower compared to the nano-sized one (Table 1, second column).

A comparison between the morphological features exhibited by the nano-sized powders, respectively known as P25 and PC105, and the micro-sized ones, indicated as 1077 and AT-1, was investigated by TEM (Fig. 2) and SEM (images not reported for the sake of brevity).

TEM images (Fig. 2) confirm the above average crystallites size extrapolated by XRD analysis also excluding the presence of ultrafine particles in both 1077 and AT-1 samples.

It can be also evidenced that the nano-sized materials perfectly fall within the "nano" definition: in fact, both samples are characterized by average particles size of 15–30 nm (see top sections in figure), closely packed features and roundish contours. In any case, the highly crystalline nature of the particles is witnessed by the incidence of fringe patterns, generated by the superimposition of crystals (mostly) belonging to the TiO$_2$ anatase polymorph. For both nano-sized samples, the most frequently observed planes ($d = 0.357$ nm) are due to the (1 0 1) family [19].

As for what concern the micro-sized materials, they are characterized by huge average dimensions of the particles: see the bottom sections of Fig. 2. This feature totally agrees again with the indications coming from XRD analysis, pointing out that both 1077 and AT-1 samples exhibit average dimensions in the 120–200 nm range. Moreover, the (1 0 1) crystal planes belonging to the TiO$_2$ anatase polymorph are also in these cases the most frequently observed, with a consequent less defective nature of the particles themselves.

The surface state of the TiO$_2$ particles was analyzed by XPS. The survey shows traces of K and P for AT-1 (5.3 and 3.4 at%, respectively), K for 1077 (3.3 at%) and S for AT-1 (1.4 at%) surely due to the starting reactants of the industrial process. No significant differences can be appreciated in the Ti 2p region among all the present samples concerning the binding energies (BE) and the full width at

half-maximum (FWHM) values. The peak Ti 2p$_{3/2}$ is always regular and the BE (forth column in Table 1) compares well with the data for Ti(IV) in TiO$_2$ materials [20]. The analysis of the oxygen peaks exhibits the presence of more than one component, which can be attributed to lattice oxygen in TiO$_2$ (529.9 eV) and to surface OH species (>531.5 eV) respectively [21]. A particular O$_{1s}$ shape was observed for PC105 (Fig. 3). In this case, the OH component is very intense probably due to a particular industrial synthesis in order to enhance the photocatalytic efficiency of the sample.

The hydrophilicity/hydrophobicity character of photocatalysts surface plays a crucial role in determining the adsorption step and thus the photocatalytic activity, at least in the degradation of pollutants [13,22]. The fifth column of Table 1 reports the OH/O$_{tot}$ surface ratio, a quantitative measure of the hydrophilicity/hydrophobicity of the TiO$_2$ surface, estimated using the XPS-determined surface OH atomic concentrations normalized by the total oxygen atomic concentrations (O$_{tot}$) [22]. P105 exhibits the highest concentration of OH that represent the 85% of the oxygen at the surface. It is noteworthy that the micro-sized samples present a higher atomic concentration of OH groups in comparison with P25, pointing out the higher hydrophilic character of their surface.

In XPS, not only the information on the BE of a specific element can be obtained but also the total density of states (DOS) of the valence band (VB) [23]. This measurement is useful to unravel the effect of TiO$_2$ structural modifications on the electronic properties of the material. For example, the insertion of non-metal elements such as N, S, C has been reported to introduce additional electronic states above the valence band edge thus creating a band-gap narrowing and a consequent shift of TiO$_2$ absorption toward the visible region [24]. In addition, when comparing semiconductor nanoparticles/microparticles the quantum size effect could play also a role, giving band-gap narrowing in the bigger sized particles in respect to the smaller ones. The VB XPS spectra of both nano-sized (a, b) and micro-sized samples (c, d) are reported in Fig. 4. The VB maximum position was determined through linear extrapolation and the same values around −2.6 eV (±0.2 eV that is inside the instrumental error) were observed for all samples, which is a typical value for TiO$_2$ [24]. The absence of additional bands above the VB in the AT-1 spectra suggests that the impurity (i.e., S) revealed by survey analysis are not inserted in the TiO$_2$ lattice.

Experimental data of diffuse reflectance were elaborated to absorption coefficient values $F(R)$ according to the Kubelka–Munk equation. The corresponding band-gap values obtained by this procedure for all samples are reported in Table 1 (sixth column). The obtained band-gap values do not exhibit large differences among the various samples and fall in the range expected for the TiO$_2$ material.

3.2. Photocatalytic activity

In order to study the photocatalytic activity of nano- and micro-sized samples, the degradation of three different VOCs: acetone, acetaldehyde and toluene has been performed.

When the photocatalyst is irradiated with energy equal to or greater than the band gap, an electron is excited from the valence band (VB) to the conduction band (CB) leaving a hole in the former. The formation of these photogenerated charges starts the
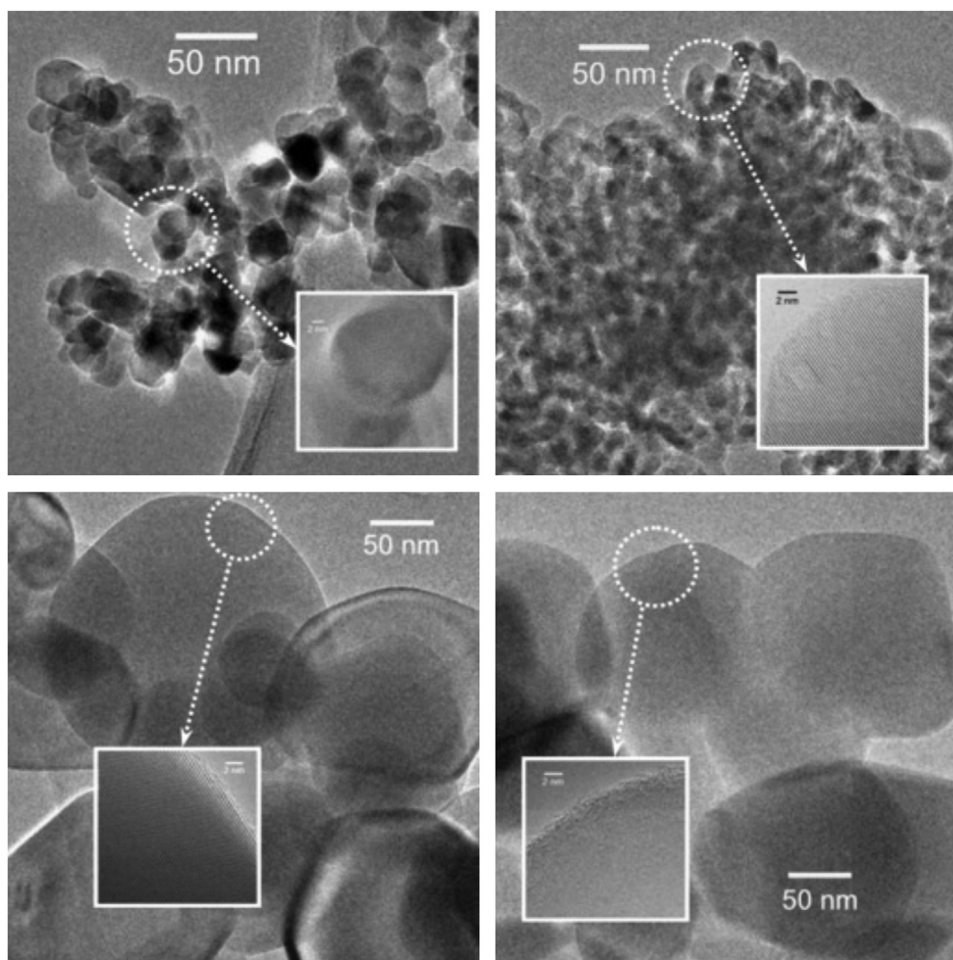
Fig. 2. Top sections: left-hand image refers to P25, right-hand image refers to PC105.　　　Bottom sections: left-hand refers to 1077, right-hand image refers to AT-1.

photocatalytic process that then proceeds through a series of complex reactions that induce the degradation of pollutants adsorbed onto the TiO_2 surface [11].

Photodegradation of both acetone and acetaldehyde, two hydrophilic and polar pollutants that usually are present in high concentration in indoor environment, was firstly investigated. Degradation percentages for different VOCs are reported in Table 2.

Acetone is a very interesting molecule from the degradative point of view because its reaction pathway passes through the formation of acetaldehyde as byproduct (Fig. 5a) as reported by Stengl et al. [25]. This hypothesis is confirmed also in our case as acetaldehyde reaction time is always lower than the acetone time for all samples (see Table 2, second and third column). In both cases, the nano-sized samples exhibit high photocatalytic efficiency, leading to the complete pollutants degradation within shorter reaction time compared to the micro-sized 1077 material. Despite the high starting pollutants concentration, for both pollutants, PC105 exhibits the best photocatalytic results with their

complete disappearance in 60 min in the case of acetone and 50 min for acetaldehyde. For P25, PC105, and 1077, CO_2 is the only byproduct of the reaction confirming the complete degradation of both acetone and acetaldehyde (depending on the reaction test) without formation of adsorbed byproducts on the samples surface (verified by FTIR measurements on the sample surface after the kinetic runs). A different behavior was achieved by AT-1 sample which exhibits an incomplete degradation of both acetone and acetaldehyde.

These results highlight that the nano-sized TiO_2 (P25 and PC105) exhibit the highest photocatalytic performances in the degradation of acetone and acetaldehyde with respect to the micro-sized ones (1077 and AT-1). Interestingly, despite the low surface area, the micro-sized sample 1077 shows an increased reaction time of only 15–30% compared to P25.

A reason for the high photocatalytic activity of PC105 could be the high OH concentration at the surface revealed by XPS that can favor the adsorption of pollutants (and intermediates of degradation) thus leading to a very active photocatalyst. However, considering only OH/O_{tot} ratio, the catalytic results presents some discrepancies. For example, micro-sized samples have higher hydrophilicity/hydrophobicity ratio than P25 but lower catalytic efficiency. On the other hand, considering surface area and particle size (see Table 1), acetone and acetaldehyde photodegradation follows the trend: the smaller is the crystallite size the faster is the photocatalytic kinetic. The growth of metal oxide (i.e., TiO_2) crystallites influence the degree of reconstruction, stoichiometry, and reactive sites (e.g., terrace, vacancies) at its surface thus driving

Table 2
Photocatalytic degradation percentages of VOCs.

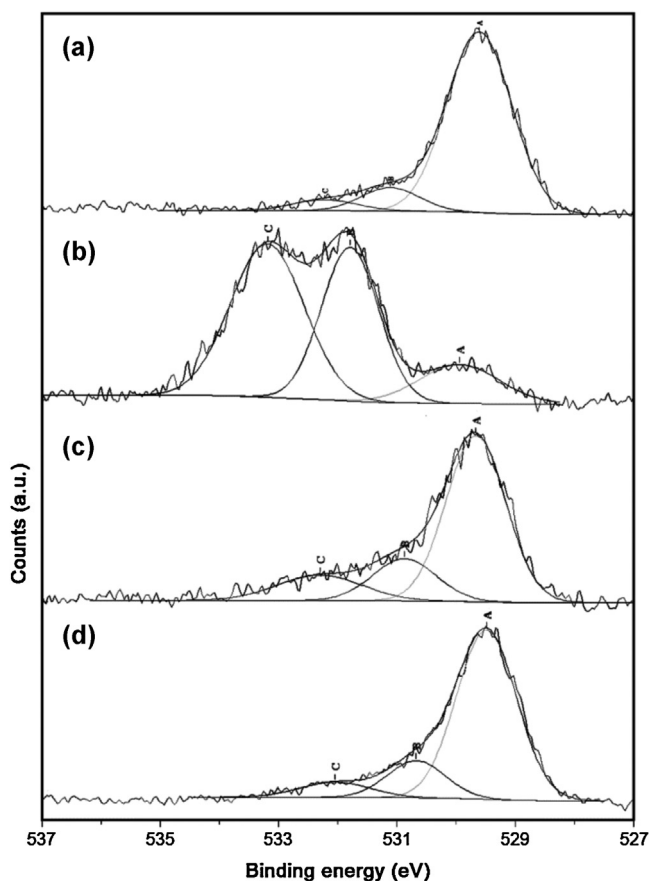| Sample	Acetone (reaction time 2 h)	Acetaldehyde (reaction time 2 h)	Toluene (reaction time 6 h)
P25	100% in 70 min	100% in 60 min	52%
PC105	100% in 60 min	100% in 50 min	50%
1077	100% in 90 min	100% in 70 min	46%
AT-1	49% after 120 min	46% after 120 min	46%

Fig. 3. O1s XPS spectra for (a) P25; (b) PC105; (c) 1077; (d) AT-1.

also the catalytic behavior. Nanocrystals should have a higher number of coordinately defects sites (i.e., steps and corner) compared to micro-sized crystals. Therefore, we think that the surface reactivity of our photocatalysts depends on the OH/O_{tot} ratio and that the importance of OH groups might be determined by the TiO_2
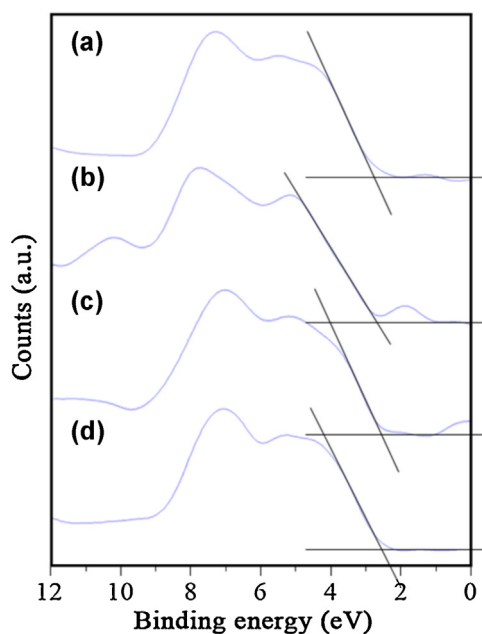

Fig. 4. VB XPS spectra along with VB maximum determining by the linear extrapolation method for (a) P25; (b) PC105; (c) 1077; (d) AT-1.

crystallite size, which in turn is induced for the different type of exposed OH reactive sites onto the surface of nano- and micro-sized TiO_2 samples.

In order to find a correlation between the samples reactivity and the type of OH reactive sites exposed at the surface of the material, a thorough study of the surface OH species by means of in situ FTIR spectroscopy has been carried out. Section (a) of Fig. 6 reports, in the ν_{OH} spectral range (3900–2800 cm^{-1}), the spectra of the various samples after prolonged outgassing at room temperature (RT). All the materials exhibit two complex absorption bands, respectively located in the 3000–3450 cm^{-1} range and at $\nu \geq 3600$ cm^{-1}. On the basis of the spectral behavior and of literature data, the first envelope can be ascribed to the ν_{OH} of all H-bonded OH groups present at the surface of the solid, whereas the second one corresponds to the stretching mode (ν_{OH}) of all Ti-OH species free from hydrogen bonding interactions [26–28]. This is not surprising, as an activation in vacuo at RT can only get rid of the physisorbed fraction of (associated/undissociated) water molecules present at the surface of the various TiO_2 systems.

The comparison between the OH profile of the different samples allows then to state that:

(i) The total amount of OH species (both free and H-bonded) present at the surface of PC105 is definitely higher than for all other TiO_2 (see curve 1), confirming the results reported in the XPS section.
(ii) The signals relative to the free OH species appear more complex in the case of the two nano-sized samples (see curve 1 and 2).

To better identify the different spectral components present at higher ν, i.e. the OH species free from hydrogen bonding interactions and thus active in the photocatalytic process, all samples have been activated in vacuo at 300 °C. This thermal treatment is able to remove the interference between the ν_{OH} signals of adsorbed water and the surface OH groups, as it should only remove the signals of adsorbed water leaving virtually unchanged the distribution of surface "free" OH species [29].

The spectra collected after such thermal treatment are reported in the blown-up section (b) of Fig. 6. It is well known from the literature [29–32] that the variety of components present in this spectral range can be related to the presence of OH groups located on sites with a different "local" structure i.e. exposed on either reactive facets and/or borders. The bands observed at $\nu \geq 3680$ cm^{-1} can be ascribed to linear (terminal) Ti-OH species, whereas the bands at lower frequencies can be related to Ti-OH-Ti bridged species.

For all samples, a specific family of bridged OH groups, located at ~3670 cm^{-1}, is predominant with respect to all the other free OH species (both linear and bridged). Still, the presence of the signal at around 3640 cm^{-1}, evident only for nano-sized TiO_2 (Fig. 6b, curve 1 and 2), except for AT-1 sample for which a very weak band is also present, highlights that the Ti-OH-Ti bridged species are located in different coordination environments. At the same way, comparing nano- (Fig. 6b, curve 1 and 2) and micro-sized (Fig. 6b, curve 3 and 4) spectra in the region at $\nu \geq 3680$ cm^{-1}, it is evident that the former are characterized by a significant higher amount of terminal Ti-OH species (see signals located at ~3717 cm^{-1}). Moreover, the direct comparison of the two micro-sized TiO_2 highlights that there is a different ratio between the family of bridged-OH species at 3670 cm^{-1} and the families of terminal OH groups located at 3723 and 3700 cm^{-1} and that this ratio is definitely higher for the 1077 sample. The detailed FTIR analysis of the ν_{OH} stretching region demonstrates that the Ti-OH-Ti bridged species play a key role in driving the photocatalytic activity of both nano- and micro-sized TiO_2. Indeed, the higher is the amount of Ti-OH-Ti bridged groups, the higher is the photocatalytic efficiency toward the degradation of acetone and acetaldehyde. On the contrary, linear Ti-OH
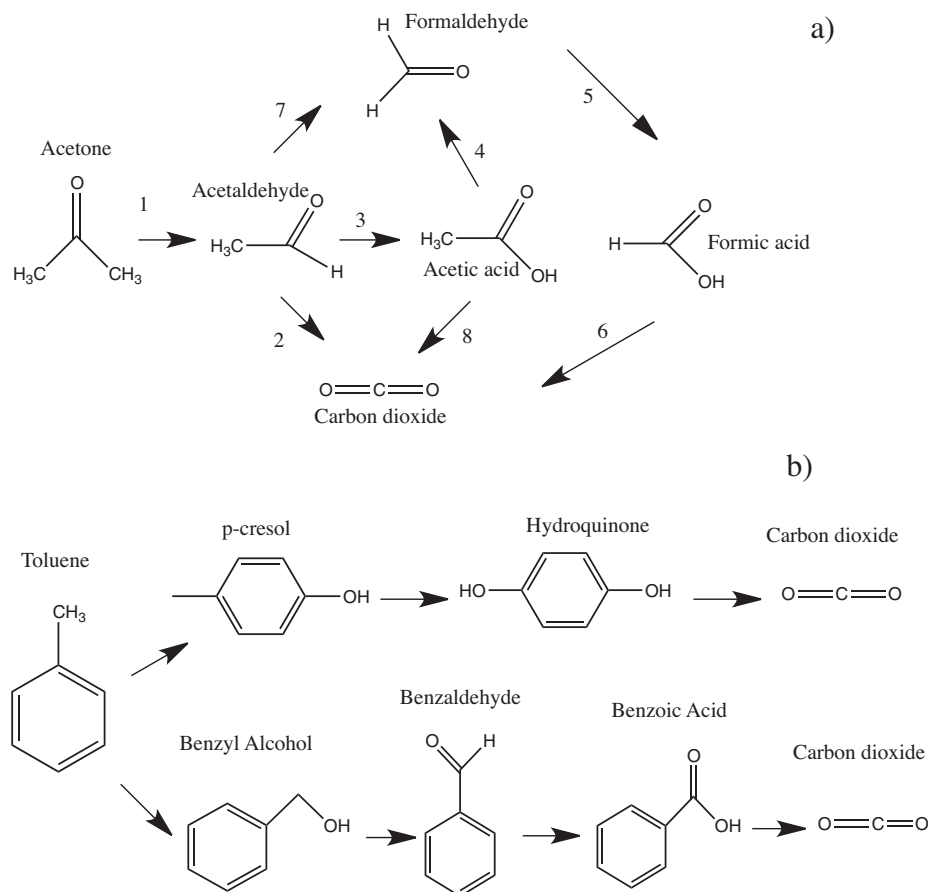
Fig. 5. Reaction pathways of photocatalytic: (a) acetone oxidation, (b) toluene oxidation.

species seems to have a less relevant impact on the samples activity. Still, the peculiar photocatalytic behavior exhibited by AT-1 sample could be explain considering that it possesses a different amount of bridged-OH species with respect to the other micro-sized sample (1077).

In order to compare the photocatalytic efficiency of nano- and micro-sized TiO_2 toward a less polar and less hydrophilic (if compared with acetone and acetaldehyde) VOC, the photodegra- dation of toluene has been performed. Toluene degradation results more difficult, mainly due to the presence of the aromatic ring. In fact, for all samples, the pollutant is not completely degraded even after 6 h of reaction (Table 2, fourth column). Moreover, it is noteworthy that the degradation percentages fall more or less in the same range (46–52%) with a slightly higher value for the P25 system.

A low amount of CO_2 formation, with respect to the degrada- tion reactions of the other two VOCs, confirms the incompleteness of the degradation reaction (Fig. 7A for 1077 and Fig. 7B reported as example). Ardizzone et al. [13] report a possible degradation scheme for toluene (Fig. 5b) in which the formation of various byproducts is evident and monitored by FTIR measurements. The authors highlighted that these species remain irreversibly adsorbed at the catalyst surface avoiding the photo-degradation reaction to continue, probably because the photoactive sites are completely covered and thus deactivated.

In the present paper, this aspect was investigated by means of FTIR measurements performed analyzing the samples surface after the kinetic run with toluene (see full curves in Fig. 8). The spectra collected on both fresh (dotted lines) and used (full lines) sam- ples are reported in Fig. 8 in the 3900–2800 cm^{-1} (section (a)) and

1800–1200 cm^{-1} (section (b)) spectral ranges. Only the spectra of one nano-sized (spectral set I) and one micro-sized (spectral set II) TiO_2 have been reported for reason of space, being the behavior of the other two materials substantially coincident.

After the employment in toluene degradation, the spectra of the materials undergo deep changes. In particular, in the
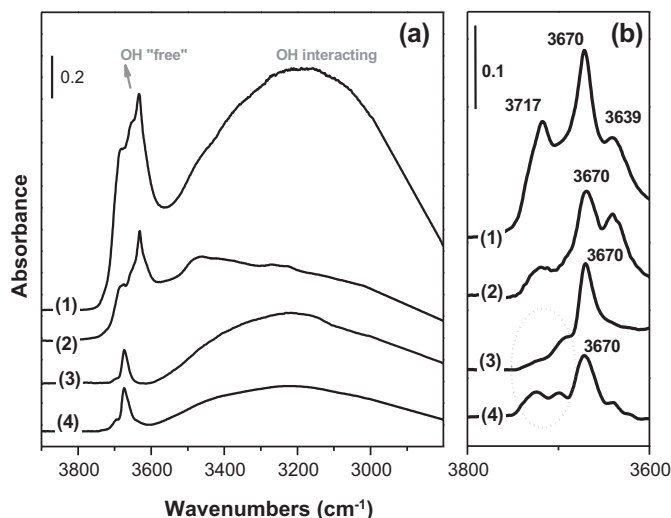

Fig. 6. Absorbance IR spectra, mass-normalized to the weight of the heaviest sam- ple, relative to the O—H stretching spectral region of samples outgassed at RT for 60 min (section (a)) and activated (in presence of O_2) at 300 °C for 60 min (section (b)): PC105 (1), P25 (2), 1077 (3), AT-1 (4).
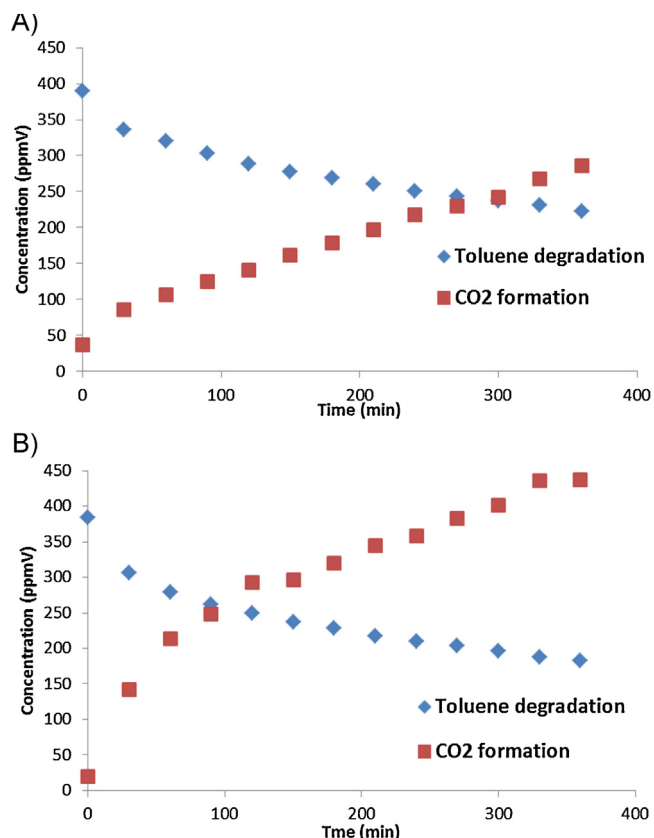
Fig. 7. CO_2 conversion and toluene degradation for A) 1077 and B) P25 samples.

3900–$2800 \, cm^{-1}$ region (see section (a) of Fig. 8), it is possible to observe:

- the total disappearance of the signals due to the stretching mode (ν_{OH}) of Ti-OH species free from hydrogen bonding interactions with the parallel increase of the broad envelope generated by H-bonded OH groups;

- the formation of a new complex of bands located in the 3150–$2850 \, cm^{-1}$ range (somehow superimposed to the envelope of interacting OH species) ascribable to the ν_{CH} stretching modes of CH-containing species of either aliphatic or aromatic nature [33].

For what concerns the low frequency region (1800–$1200 \, cm^{-1}$ range, see section (b) of Fig. 8), new intense and well defined components appear in the spectrum. These bands can be ascribed to the formation of new adsorbed surface species generated during toluene degradation, as reported in the reaction profile of Fig. 5b. In particular, it is possible to recognize signals of unreacted toluene (T) and of several by-products deriving from its degradation, among which benzyl alcohol (BZOH), benzoic acid (BZAc) and benzaldehyde (BZH) [13,33].

On the basis of all the previous results, it is possible to state that the catalysts surface undergoes irreversible changes after the employment in the photodegradation reaction of toluene: the photo-active "free" Ti-OH sites are completely absent, as a result of their participation to the reaction. Their disappearance is a clear evidence of why toluene degradation appears incomplete even after 6 h of reaction for all the samples, regardless of the morphological features of the materials.

Therefore, in the case of toluene and in general for all less hydrophilic VOCs, it is well evident that both micro-sized materials and nano-sized ones possess almost the same photocatalytic behavior.

The OH/O_{tot} ratio, as obtained by elaboration of the O 1s XPS peak (Table 1, fifth column), is generally considered to be a measure of the hydrophilicity/hydrophobicity of an oxide [34] and seems to be a key factor to explain the nanomaterials behavior. In the present case, the nano-sized samples seem to be very different, as the OH/O_{tot} values for the PC105 material is much higher than that reported for P25 and this difference is due to the presence of a very intense OH peak for PC105. An efficient adsorption of the pollutant molecule at the semiconductor surface may promote the photocatalytic reaction: as a consequence, the adsorption of acetone/acetaldehyde or toluene on TiO_2 surface has been demonstrated to be a crucial point in affecting the subsequent photocatalytic efficiency [13].
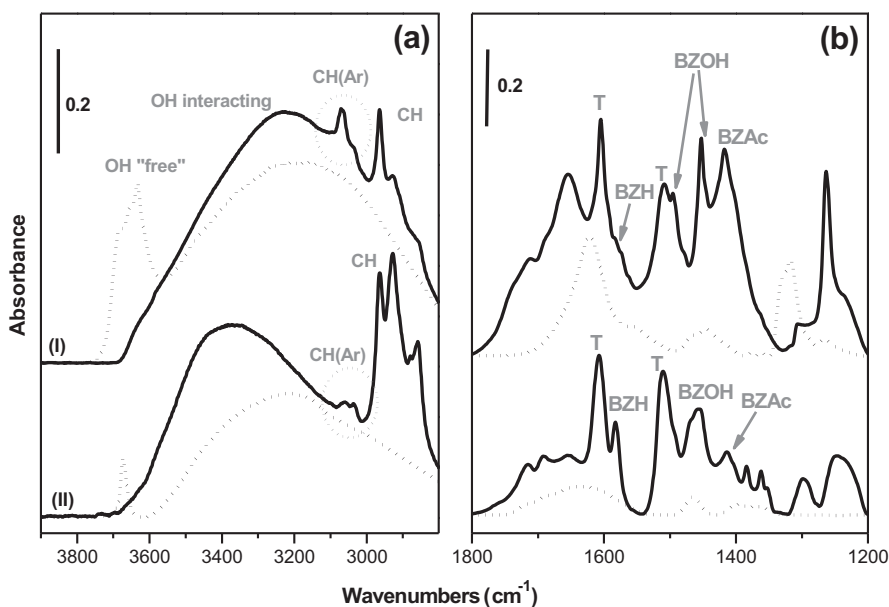

Fig. 8. Absorbance IR spectra in the 3900–$2800 \, cm^{-1}$ (section (a)) and 1800–$1200 \, cm^{-1}$ (section (b)) spectral regions of fresh (dotted lines) and used in toluene degradation reaction (full lines) samples. Spectral set I: nano-sized PC105. Spectral set II: micro-sized 1077. The abbreviations T, BZH, BZOH and BZAc are explained in the text.

4. Conclusion

The present paper compares the photocatalytic performance of four commercial TiO_2 powders, two nano-sized and two micro-sized materials, in the degradation of three important VOCs, representative of the indoor pollution.

An efficient adsorption of the pollutant molecule at the semi-conductor surface promotes the photocatalytic reaction. As a consequence, the adsorption of acetone/acetaldehyde or toluene on TiO_2 surface has been demonstrated to be a crucial point in affecting the subsequent photocatalytic activity. In particular, FTIR analysis of the ν_{OH} stretching region demonstrated that the Ti-OH-Ti bridged species play a key role in driving the photocatalytic activity of both nano- and micro-sized TiO_2. Indeed, the higher is the amount of Ti-OH-Ti bridged groups, the higher is the photocatalytic efficiency toward the degradation of acetone and acetaldehyde.

Among the different TiO_2, PC105 sample exhibits the best results for both acetone and acetaldehyde photodegradation. On the contrary, in the case of less hydrophilic VOCs, it is well evident that both micro-sized and nano-sized materials possess almost the same photocatalytic behavior. In fact, the catalysts surface seems to undergo irreversible changes after the employment in the photodegradation reaction of toluene. In particular, after the contact with toluene, the photo-active "free" Ti-OH sites totally disappear, as a result of their participation to the reaction, explaining why toluene degradation appears incomplete even after 6 h of reaction for all the samples, regardless of the morphological features of the materials.

Finally, it is important to highlight that the present study allowed to demonstrate that micro-sized TiO_2 are very promising materials to be employed in the photocatalytic degradation of VOCs, so limiting the possible risks for the human health deriving by the use of nanoparticles.

References

[1] S.M. Gupta, M. Tripathi, Central European Journal: Chemistry 10 (2012) 279–294.
[2] X. Wang, Y. Liu, Z. Hu, Y. Chen, W. Liu, G. Zhao, Journal of Hazardous Materials 169 (2009) 1061–1067.
[3] D.P. Macwan, P.N. Dave, S. Chaturvedi, Journal of Materials Science 46 (2011) 3669–3686.
[4] S.A. Love, M.A. Maurer-Jones, J.W. Thompson, Y-S. Lin, Annual Review of Analytical Chemistry 5 (2012) 181–205.
[5] S. Park, S. Lee, B. Kim, S. Lee, J. Lee, S. Sim, M. Gu, J. Yi, J. Lee, Biotechnology and Bioprocess Engineering 17 (2) (2012) 276–282.
[6] O. Creutzenberg, Inorganic Compounds 86 (2012) 1117–1122.
[7] B.J. Panessa-Warren, J.B. Warren, S.S. Wong, J.A. Misewich, Journal of Physics: Condensed Matter 18 (2006).
[8] E. Brun, M. Carriere, A. Mabondzo, Biomaterials 33 (2012) 886–896.
[9] C.J. Green, S. Ndegwa National Collaborating Centre for Environmental Health (2011).
[10] C. Schulze, A. Kroll, C.M. Lehr, U.F. Schäfer, K. Becker, J. Schnekenburger, C.S. Isfort, R. Landsiedel, W. Wohleben, Nanotoxicology 2 (2008) 51–61.
[11] S. Kwon, M. Fan, A.T. Cooper, H. Yang, Critical Reviews in Environment Science and Technology 38 (2008) 197–226.
[12] L. Yang, B.J. Kruse, Optical Society of America A 21 (2004) 1933–1941.
[13] S. Ardizzone, C.L. Bianchi, G. Cappelletti, A. Naldoni, C. Pirola, Environmental Science & Technology 42 (2008) 6671–6676.
[14] C.L. Bianchi, C. Pirola, E. Selli, S. Biella, Journal of Hazardous Materials 211–212 (2012) 203–207.
[15] C.H. Ao, S.C. Lee, C.L. Mak, L.Y. Chan, Applied Catalysis B 42 (2003) 119–129.
[16] J. Jeong, K. Sekiguchi, K. Sakamoto, Chemosphere 57 (2004) 663–671.
[17] M. Addamo, V. Augugliaro, S. Coluccia, A. Di Paola, E. Garcia-Lopez, V. Loddo, G. Marcì, G. Martra, L. Palmisano, International Journal of Photoenergy (2006) 1–12.
[18] G. Marcì, M. Addamo, V. Augugliaro, S. Coluccia, E. Garcia-Lopez, V. Loddo, G. Martra, L. Palmisano, M. Schiavello, Journal of Photochemistry and Photobiology A 160 (2003) 105–114.
[19] ICDD anatase file no. 21-1272.
[20] G. Cappelletti, C.L. Bianchi, S. Ardizzone, Applied Surface Science 253 (2006) 519–524.
[21] S. Ardizzone, C.L. Bianchi, G. Cappelletti, S. Gialanella, C. Pirola, V. Ragaini, Journal of Physical Chemistry C 111 (2007) 13222–13231.
[22] A. Naldoni, C.L. Bianchi, C. Pirola, K.S. Suslick, Ultrasonics Sonochemistry 20 (2013) 445–451.
[23] A. Naldoni, M. Allieta, S. Santangelo, M. Marelli, F. Fabbri, S. Cappelli, C.L. Bianchi, R. Psaro, V. Dal Santo, Journal of the American Chemical Society 134 (2012) 7600–7603.
[24] X. Chen, C. Burda, Journal of the American Chemical Society 130 (2008) 5018–5019.
[25] V. Stengl, V. Houskova, S. Bakardjieva, N. Murafa, New Journal of Chemistry 34 (2010) 1999–2005.
[26] L.H. Little, Infrared Spectra of Adsorbed Species, Academic Press, London, 1966.
[27] C. Morterra, Faraday Transactions 1 84 (5) (1988) 1617–1637.
[28] C. Morterra, V. Bolis, E. Fisicaro, Colloids and Surfaces 41 (1989) 177–188.
[29] M. Minella, M.G. Faga, V. Maurino, C. Minero, E. Pelizzeti, S. Coluccia, G. Martra, Langmuir 26 (2010) 2521–2527.
[30] M. Primet, P.P. Pichat, M.V. Mathieu, Journal of Physical Chemistry 75 (1971) 1216–1220.
[31] A.A. Tsyganenko, V.N. Filimonov, Journal of Molecular Structure 19 (1973) 579–589.
[32] C. Deiana, E. Fois, S. Coluccia, G. Martra, Journal of Physical Chemistry C 114 (2010) 21531–21538.
[33] N.B. Colthup, L.H. Daly, S.E. Wiberley, Introduction to Infrared and Raman Spectroscopy, 2nd ed., Academic Press, New York, 1975.
[34] R. Inaba, T. Fukahori, M. Hamamoto, T. Ohno, Journal of Molecular Catalysis A: Chemical 260 (2006) 247–254.